

Computational Exploration of the Nanogold Energy Landscape

Michael McGuigan
and
J.W. Davenport
Brookhaven National Laboratory
Upton NY 11973
mcguigan@bnl.gov

Abstract

We use density functional theory to quantify finite size and shape effects for gold nanoclusters. We concentrate on the computation of binding energy as a function of bond length for icosahedral and cuboctohedral clusters. We find that the cuboctohedral gold clusters have lower energy for 13 atoms. For 55 atoms we find that the icosahedral gold clusters have lower binding energy. We also introduce a one parameter family of geometries that interpolate between the icosahedral and cuboctohedral clusters that is parametrized by an angle variable. We determine the binding energy dependence on shape as a function of the angle variable for 13 and 55 atom clusters with a minimum at the cuboctohedral point and icosahedral point respectively. We also compute the binding energy for the 147 atom gold nanocluster and show that the binding energy of the icosahedral cluster is lower than the 147 atom cuboctohedral gold cluster. We also compute the binding energy of the $Au_{55}O_2$ molecule with possible applications to catalysis.

1 Introduction

An important application area for nanoscience are gold nanoclusters. These clusters can be used in energy science as catalysts and in medicine for drug delivery. It is also important to understand the basic physics and chemistry of gold nanoclusters to understand the limitations of the current applications as well as to suggest new ones. Experiments on gold nanoclusters have recently been performed on clusters with 102 gold atoms [1]. In addition increasing computational power has led to the ability to simulate a nanocluster of hundreds of atoms on supercomputers running

scalable density functional codes. Thus this is an exciting time in the development of nanoscience where computation, theory, and experiment are helping to improve our understanding of these systems.

The main tool that we use to computationally probe gold nanoclusters is density functional theory run on large parallel computers. Density functional theory is a computationally efficient approach to many body systems that maps the interacting many body Schrodinger equation to a single body noninteracting problem given by:

$$\left(-\frac{\hbar^2}{2m}\nabla^2 + V_s(\vec{r})\right)\psi_i(\vec{r}) = \epsilon_i\psi_i(\vec{r})$$

where V_s is defined by:

$$V_s(\vec{r}) = V_{ext}(\vec{r}) + \int \frac{e^2 n(\vec{r}')}{|\vec{r} - \vec{r}'|} d^3 r' + V_{XC}[n(\vec{r})]$$

with $V_{ext}(\vec{r})$ the external potential, $V_{XC}[n(\vec{r})]$ the exchange correlation potential and $n(\vec{r})$ the electron density.

One typically uses a local density approximation and generalized gradient approximation where the exchange functional is a local function of the density and gradient of the density. One then iteratively solves the one-body equation using the relation between the electron wave function and density to evaluate the exchange correlation potential. More details about the density functional approach can be found in many textbooks, for example [2].

Density functional theory has been implemented in several quantum chemistry codes. In this paper we use the NWChem quantum chemistry code distributed by PNNL [3]. We also use a large Blue Gene L parallel supercomputer that efficiently runs NWChem up to 2048 nodes or 4096 processors. A general description of the application of NWChem to materials science can be found in [4]. Outstanding features of the NWChem input file specify the geometry, basis, effective core potential, exchange and correlation functionals, DIRECT, SMEAR and MULT. We used the basis set specified by SBKJC VDZ ECP [5] and the pbe exchange and correlation functionals [6]. The DIRECT keyword indicates that all integrals are computed on the fly, the SMEAR keyword allows fractional occupation of molecular orbitals, and the MULT keyword defines the spin multiplicity [7]. In this paper we used the default smear value of .001 and multiplicity 2.

Besides the practical application of gold nanoclusters little is known of the structure of the energy landscape of these systems even though the chemistry and material properties strongly depend on the position in this landscape. The main difficulty is that even with 13 atoms one has a 13×3 dimensional space to explore and this is difficult computationally as well as difficult to visualize. Thus the main purpose

of this paper is to find a simpler description of this landscape in terms of the size and shape of the gold nanoparticles for well known structures like the icosahedron and cuboctahedron. Previous density functional studies of gold nanoparticles are given by [8], [9], [10], [11], [12]. In particular [8] and [9] studied the relative energy between icosahedral and cuboctahedral gold clusters and our results are consistent with their results. The nanogold phase map in temperature and critical size has recently been determined based on relativistic ab initio calculation and verified using high resolution electron microscopy at finite temperature [13]. Their work indicates that different shapes of nanoparticle are more stable depending on the place in the phase diagram. By varying the size and shape of the gold naocluster we are able to determine the stable configurations as a function of critical size using density functional methods at zero temperature.

For gold, relativistic effects are very important. In [14] density functional studies indicate a qualitative difference between 55 atom gold and silver nanoclusters, and found gold nanoclusters have several low-lying low-symmetry structures and washed-out electron shell structure [14]. In [15] photo-electron spectroscopy and first principle calculations indicate a nonicosahedral disordered cluster with strong surface contractions due to relativistic effects. In this paper we use an exchange potential that includes relativistic effects. However we focus on two well known structures cubocahedral and icosahedral. This leaves aside the question of the true lowest energy state of the system, but allows us to study the relative stability of the two structures as well as the transition and intermediate geometries between the icosahedron and cuboctahedron. These type of Mackay transitions between different shapes have been studied for lead [16] and iron [17] and we extend this analysis to gold nanoclusters here.

This paper is organized as follows. In section 2 we present the computation of the energy of 13 atom gold clusters in the shape of a cuboctahedron and icosahedron as well as intermediate structures. We derive a potentials which describes the dependence of the energy on the size and shape of the system. In section 3 we do the same thing for 55 atom gold clusters and compare with the previous section. We find that the cuboctahedron is more stable than the icosahedron for 13 atoms while the icosahedron is more stable than the cuboctahedron for 55 atoms. In section 4 we study the binding energy of the $Au_{55}O_2$ molecule and applications to oxidation and catalysis. We calculate the potential associated with the separation of the two oxygens and show that the presence of the gold nanoparticle lowers the potential relative to the free O_2 . In section 5 we state the main conclusions of the paper.

Table 1: Number of atoms N for a cuboctahedron or icosahedron for integer K which is the shell index.

K	N
2	13
3	55
4	147
5	309

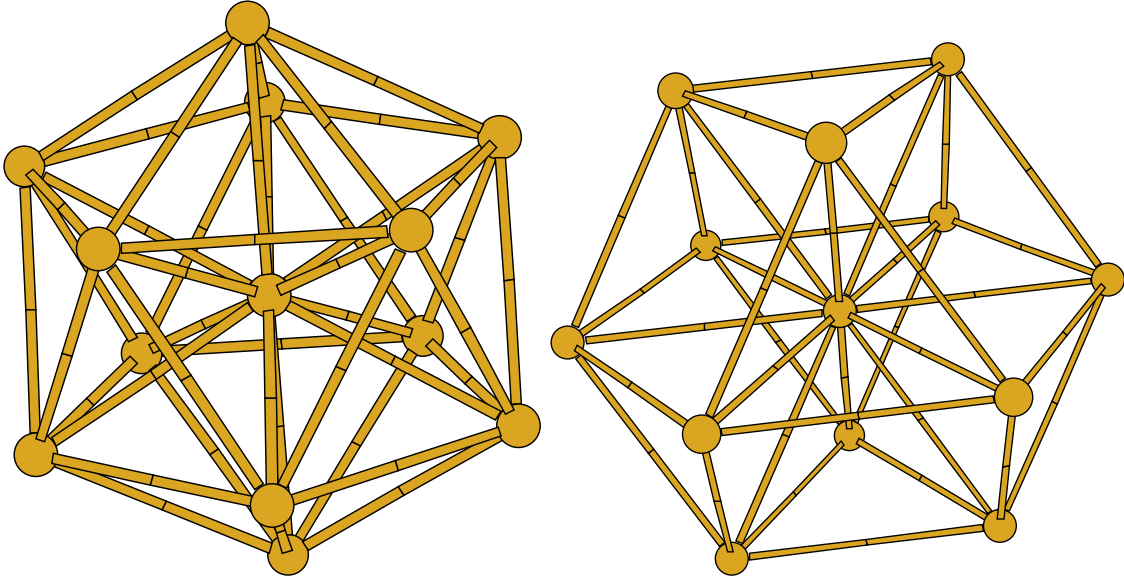


Figure 1: 13 gold atom nanocluster in the shape of an icosahedron (left) and cuboctahedron (right).

2 Finite size and shape effects in 13 atom gold nanoclusters

In density functional theory (dft) one usually computes the energy E of the multiple atom system and derives the binding energy V from:

$$V = E - NE_{atom}$$

where N is the the number of atoms and E_{atom} is the dft computation of the energy of a single gold atom.

The total number of atoms in a cuboctahedron or icosahedron N is given by [18]:

$$N = \frac{10}{3}K^3 - 5K^2 + \frac{11}{3}K - 1$$

In Table 1 we list the first few values of N for integer K which is the shell index.

We show the 13 atom icosahedral and cuboctahedral geometry in Figure 1. For the case of $K = 2$ and $N = 13$ we list the coordinates for the cuboctahedron in table

Table 2: Coordinates for 13 gold nanoclusters with bond length a and shape of cuboctahedron, icosahedron and intermediate structure with shape parameter θ .

cuboctahedron	icosahedron	intermediate
$a\frac{1}{\sqrt{2}}(0, 1, 1)$	$a\frac{1}{2}(0, 1, \varphi)$	$a(0, \cos \theta, \sin \theta)$
$a\frac{1}{\sqrt{2}}(0, -1, 1)$	$a\frac{1}{2}(0, -1, \varphi)$	$a(0, -\cos \theta, \sin \theta)$
$a\frac{1}{\sqrt{2}}(0, 1, -1)$	$a\frac{1}{2}(0, 1, -\varphi)$	$a(0, \cos \theta, -\sin \theta)$
$a\frac{1}{\sqrt{2}}(0, -1, -1)$	$a\frac{1}{2}(0, -1, -\varphi)$	$a(0, -\cos \theta, -\sin \theta)$
$a\frac{1}{\sqrt{2}}(1, 1, 0)$	$a\frac{1}{2}(1, \varphi, 0)$	$a(\cos \theta, \sin \theta, 0)$
$a\frac{1}{\sqrt{2}}(-1, 1, 0)$	$a\frac{1}{2}(-1, \varphi, 0)$	$a(-\cos \theta, \sin \theta, 0)$
$a\frac{1}{\sqrt{2}}(1, -1, 0)$	$a\frac{1}{2}(1, -\varphi, 0)$	$a(\cos \theta, -\sin \theta, 0)$
$a\frac{1}{\sqrt{2}}(-1, -1, 0)$	$a\frac{1}{2}(-1, -\varphi, 0)$	$a(-\cos \theta, -\sin \theta, 0)$
$a\frac{1}{\sqrt{2}}(1, 0, 1)$	$a\frac{1}{2}(\varphi, 0, 1)$	$a(\sin \theta, 0, \cos \theta)$
$a\frac{1}{\sqrt{2}}(1, 0, -1)$	$a\frac{1}{2}(\varphi, 0, -1)$	$a(\sin \theta, 0, -\cos \theta)$
$a\frac{1}{\sqrt{2}}(-1, 0, 1)$	$a\frac{1}{2}(-\varphi, 0, 1)$	$a(-\sin \theta, 0, \cos \theta)$
$a\frac{1}{\sqrt{2}}(-1, 0, -1)$	$a\frac{1}{2}(-\varphi, 0, -1)$	$a(-\sin \theta, 0, -\cos \theta)$
$a\frac{1}{\sqrt{2}}(0, 0, 0)$	$a\frac{1}{2}(0, 0, 0)$	$a(0, 0, 0)$

Table 3: Data near the minimum of the binding potential for 13 atom gold nanoclusters.

shape	bond length [nm]	Binding Energy [eV]
cuboctahedron	0.276897	-25.1064
cuboctahedron	0.280639	-25.3946
cuboctahedron	0.28438	-25.5349
cuboctahedron	0.288122	-25.4893
icosahedron	0.285756	-24.1683
icosahedron	0.291047	-24.5989
icosahedron	0.296339	-24.6706
icosahedron	0.301631	-24.4062

2 with bond length a . We list the coordinates for the 13 atom icosahedron also in table 2. Here $\varphi = \frac{1+\sqrt{5}}{2}$ is the golden ratio which is approximately 1.618033988749895. For the icosahedron there are two bond lengths, a and approximately $0.951057a$ and we use the former. One can also consider intermediate shapes parametrized by a shape parameter θ whose coordinates are given in Table 2. Here $\theta = 45^\circ$ corresponds to the cuboctahedron and $\theta = \arctan \varphi \approx 58.282525589^\circ$ corresponds to the icosahedron. The list of coordinates for intermediate geometries is given in the third column of Table 2.

In this paper we primarily study $K = 2$ and $K = 3$ which corresponds to 13 and 55 gold atoms respectively. Higher values of K can also be studied and require large computational resources and scalable density functional codes. In section 3 we present some results for $K = 4$ and 147 gold atoms.

Figure 2 shows the binding potential for the cuboctahedron and icosahedron

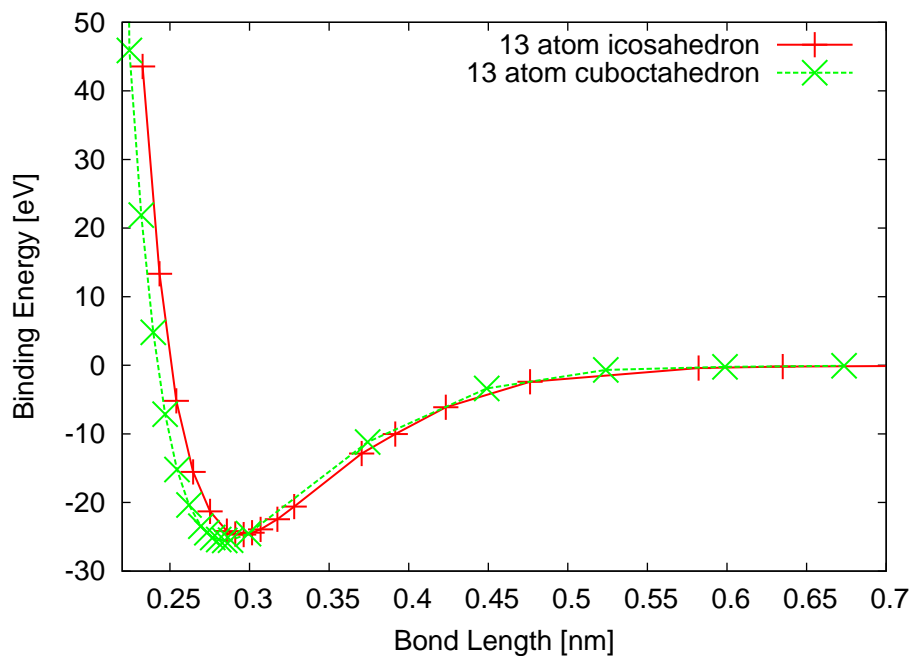


Figure 2: Binding energy as a function of bond length for 13 atom gold nanoclusters shaped like an icosahedron and cuboctahedron.

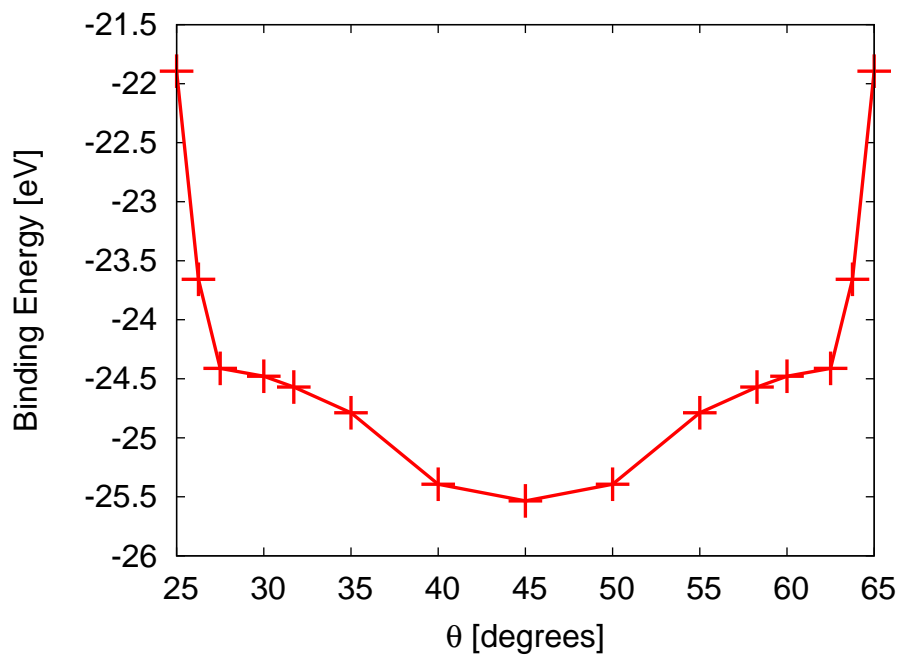


Figure 3: Binding energy as a function of the shape parameter θ for a 13 atom gold cluster. The minimum occurs at 45 degrees which corresponds to the shape of a cuboctahedron.

Table 4: Coordinates for 55 gold nanoclusters with bond length a and shape of cuboctahedron, icosahedron and intermediate structure with shape parameter θ . Here n is the number of atoms in each class of coordinates.

cuboctahedron	icosahedron	intermediate	n
13 atom cuboctahedron	13 atom icosahedron	13 atom intermediate	13
same as above scaled by 2	same as above scaled by 2	same as above scaled by 2	12
$a\frac{1}{\sqrt{2}}(\pm 2, 0, 0)$	$a\frac{1}{2}(\pm 2\varphi, 0, 0)$	$a(\pm 2\sin\theta, 0, 0)$	2
$a\frac{1}{\sqrt{2}}(0, \pm 2, 0)$	$a\frac{1}{2}(0, \pm 2\varphi, 0)$	$a(0, \pm 2\sin\theta, 0)$	2
$a\frac{1}{\sqrt{2}}(0, 0, \pm 2)$	$a\frac{1}{2}(0, 0, \pm 2\varphi)$	$a(0, 0, \pm 2\sin\theta)$	2
$a\frac{1}{\sqrt{2}}(\pm 2, \pm 1, \pm 1)$	$a\frac{1}{2}(\pm(1+\varphi), \pm\varphi, 1)$	$a(\pm(\cos\theta + \sin\theta), \pm\sin\theta, \pm\cos\theta)$	8
$a\frac{1}{\sqrt{2}}(\pm 1, \pm 2, \pm 1)$	$a\frac{1}{2}(\pm 1, \pm(1+\varphi), \pm\varphi)$	$a(\pm\cos\theta, \pm(\cos\theta + \sin\theta), \pm\sin\theta)$	8
$a\frac{1}{\sqrt{2}}(\pm 1, \pm 1, \pm 2)$	$a\frac{1}{2}(\pm\varphi, \pm 1, \pm(1+\varphi))$	$a(\pm\sin\theta, \pm\cos\theta, \pm(\cos\theta + \sin\theta))$	8

structure. The difference in the potentials is rather small so we list the values near the bottom of the potential in Table 3. From Table 3 we see that the binding energy of the cuboctahedron shape for 13 gold atoms, -25.5349 eV, is greater in magnitude than that of the icosahedron, which was -24.6706 eV. Thus our calculations indicate that the cuboctahedron is more stable than the icosahedron for 13 gold atoms. The binding energy of the cuboctahedron shape minus the binding energy for the icosahedron shape for 13 gold atoms is $\Delta E = -.8643$ eV. This is in agreement with [8] [9]. Figure 3 shows the dependence of the energy on the shape parameter θ . The potential shows a minimum at $\theta = 45$ degrees which corresponds to the cuboctahedron. Thus the cuboctahedron is stable with respect to shape transformations relative to the icosahedron. Indeed from the figure the icosahedron is not a local minimum and is unstable with respect to shape perturbations for the 13 atom gold nanocluster.

3 Finite size and shape effects for 55 atom gold nanoclusters

One can proceed in a similar manner for the 55 atom gold cluster. The cuboctahedron and icosahedron 55 atom gold nanocluster are shown in Figure 4 and coordinates are given in Table 4. The binding energy a function of bond length is shown in Figure 5 and Table 5 for the cuboctahedron and icosahedron respectively. The data indicates that the icosahedron is lower in energy than the cuboctahedron with $\Delta E = E_{cuboctahedron} - E_{icosahedron} = 1.28019$ eV.

In order to further examine the stability of 55 atom gold clusters with respect to change in shape we plot the binding energy as a function of the shape parameter θ in figure 8. The angle θ is defined similar to the 13 atom case as being 45 degrees for the cuboctahedron, $\arctan\varphi$ for the icosahedron and intermediate values in between. A

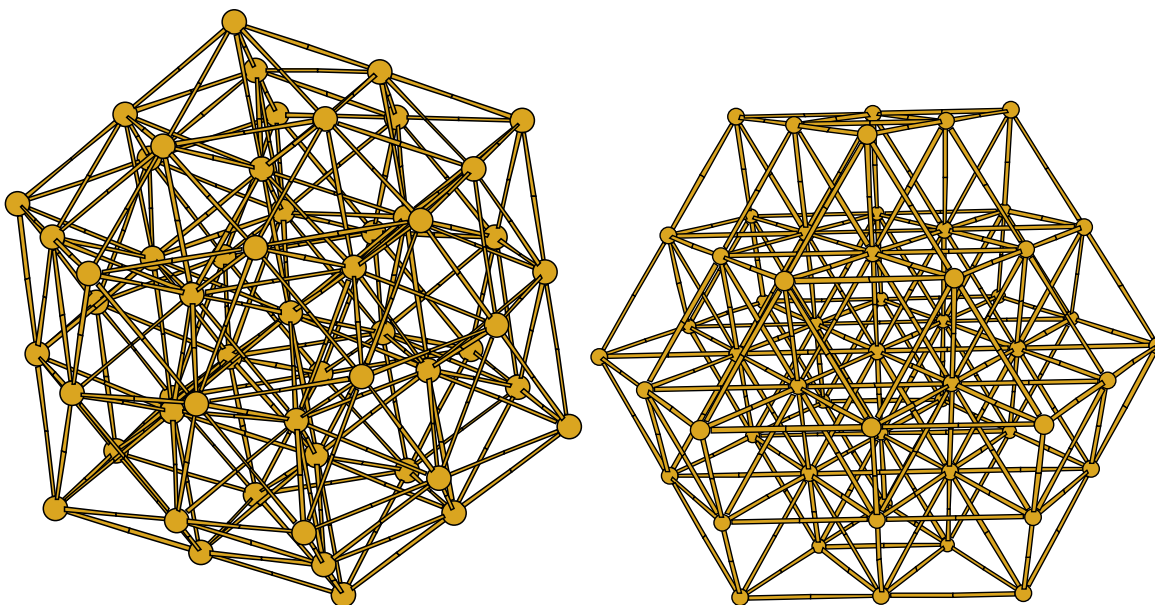


Figure 4: 55 gold atom nanocluster in the shape of an icosahedron (left) and cuboctahedron (right).

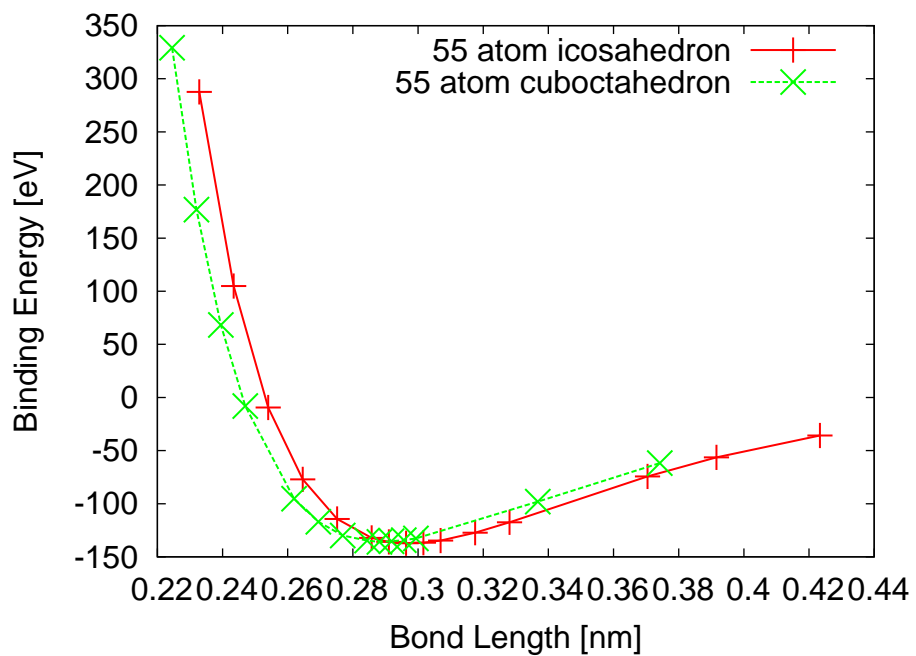


Figure 5: Binding energy as a function of the bond length for a 55 atom gold cluster.

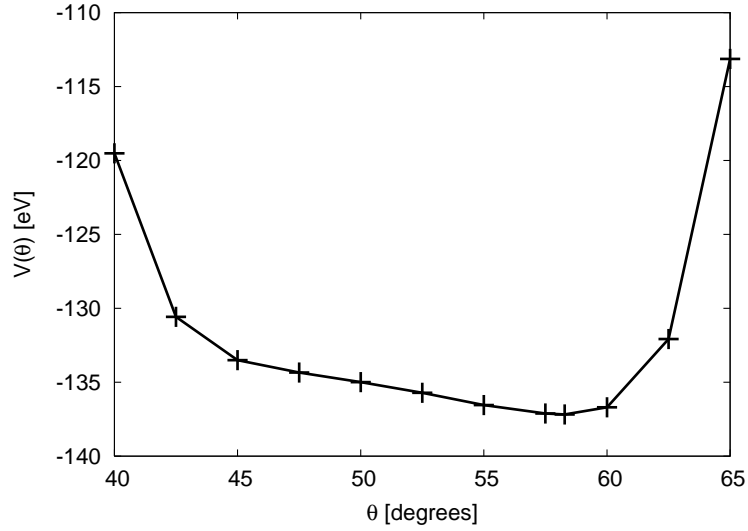


Figure 6: Binding energy as a function of the shape parameter θ for a 55 atom gold cluster. The minimum occurs at 58.282525589 degrees which corresponds to the shape of a icosahedron.

Table 5: Data near the minimum of the binding potential for 55 atom gold nanoclusters.

shape	bond length [nm]	Binding Energy [eV]
cuboctahedron	0.276897	-129.961
cuboctohedron	0.288122	-135.901
cuboctohedron	0.291864	-135.319
cuboctohedron	0.299348	-132.635
icosahedron	0.285756	-132.143
icosahedron	0.291047	-135.901
icosahedron	0.296339	-137.181
icosahedron	0.301631	-136.643
icosahedron	0.306923	-134.659

Table 6: Data near the minimum of the binding potential for 147 atom gold nanoclusters.

shape	bond length [nm]	Binding Energy [eV]
cuboctahedron	0.28438	-383.226
cuboctohedron	0.288122	-387.14
cuboctohedron	0.291864	-387.988
cuboctohedron	0.295606	-386.206
icosahedron	0.291047	-385.21
icosahedron	0.296339	-391.058
icosahedron	0.301631	-391.033

simple prescription to define the shape parameter is to replace the occurrence of the golden ratio φ in the list of icosahedral coordinates with $\tan\theta$ and scale all the 55 coordinates proportional to $\cos\theta$ to construct the interpolating nanostructures. The same prescription works also for the 13 atom case as indicated in tables 2-4. The inner bond length for the 55 atom case is fixed at $0.951057a_0$ where $a_0 = 0.296339$ nm. The resulting plot indicates the the icosahedral structure is at lower energy than the cuboctahedral structure for nanoclusters consisting of 55 gold atoms with respect to change of shape.

It should be emphasized however that we have just investigated the relative stability between two well known structures, the cuboctahedron and the icosahedron. There are many more structures that do not fit into these categories or even the interpolation between them. Some of these have lower energy [19]. Nevertheless the ability to computationally determine the potentials for size and shape of nanoclusters gives a first simplified look at the so called energy landscape of theses models. The demonstration of the ability to use efficient density functional codes and parallel computing to map out this landscape is one of the main results of this paper.

One can extend the results of this paper to larger gold clusters. Table 6 shows the results of a binding energy calculations of 147 atom gold clusters. The table indicates that for the 147 gold atom case the icosahedron is lower in energy than the cuboctahedron with $\Delta E = E_{cuboctahedron} - E_{icosahedron} = 3.07$ eV.

4 Calculation of $Au_{55}O_2$ binding energy

Besides pure gold clusters another area of interest is the use of gold clusters as oxygen catalyts involving the disassociation of O_2 molecules.

In [24] X-ray spectroscopy was used to show that 55 atom gold clusters have a maximum oxidation resistance and suggests that they may be effective oxidation catalyts. In [25] hybrid density functional calculations were done which suggests that the surfaces of small gold clusters are active sites for catalytic interactions. Among various systems they studied $Au_{13}O_2$ clusters. In [22] electronic structure of 55 atom gold nanoparticles and catalytic activity from the modified electronic structure for small nanoclusters (~ 1.4 nm). In [23] density functional calculations of Au_{55} clusters were shown not to dissociate O_2

To study these effects we calculated the binding energy of the $Au_{55}O_2$ composite system using NWChem. The $Au_{55}O_2$ molecule is shown in Figure 7. The results for the binding potential are shown in Figure 8 and 9. These figures plot the energy as a function of the distance of the center of mass of the O_2 along the x axis using the coordinates of Au_{55} from Table 4. Figure 8 shows a very flat potential away from .8 nm so we show an expanded version of the potential in figure 9 from .805 to .845 nm. This shows a minimum at .815 nm and a weak binding energy of

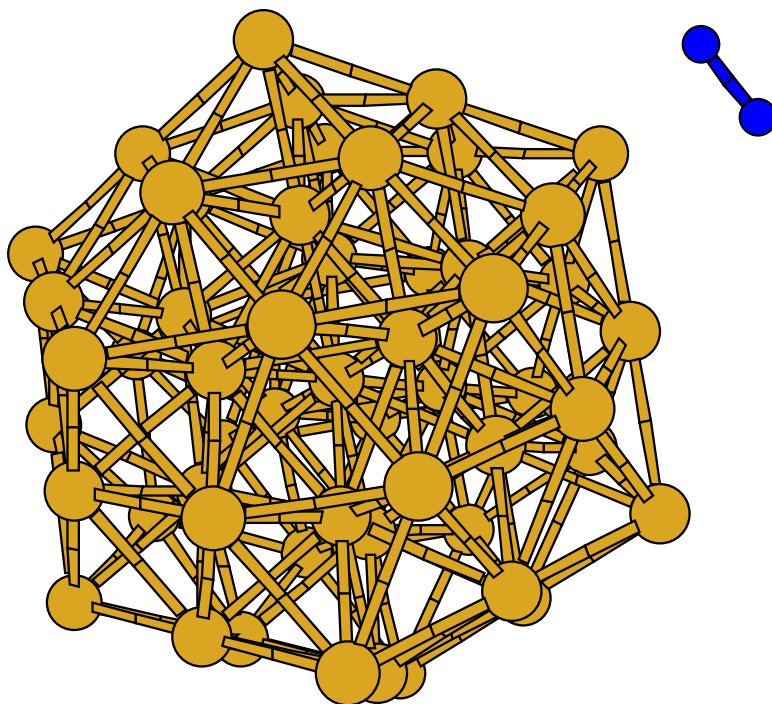


Figure 7: A 55 atom gold icosahedron nanoparticle interacting with O_2 .

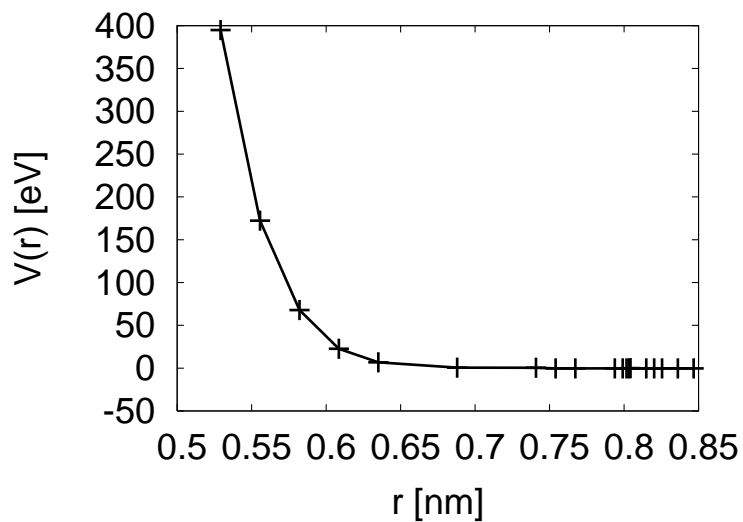


Figure 8: Binding energy as a function of the distance to the center of mass of the O_2 molecule to the center of mass of the Au_{55} nanoparticle along the x axis between .5 and .85 nm.

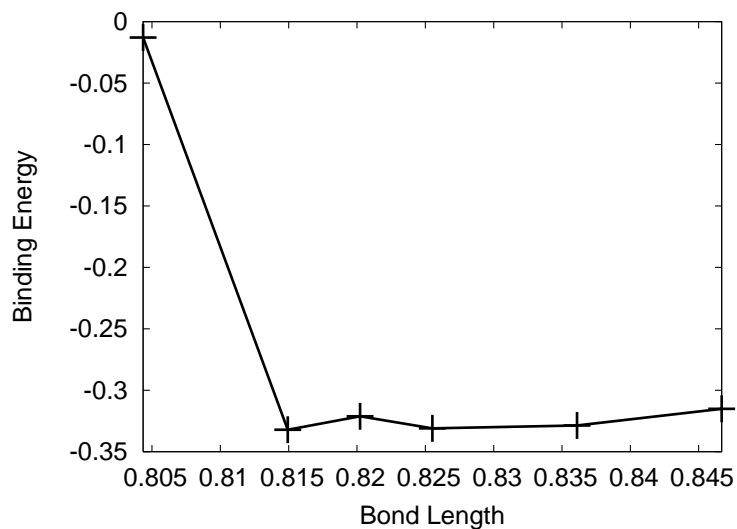


Figure 9: Binding energy as a function of the distance to the center of mass of the O_2 molecule to the center of mass of the Au_{55} nanoparticle along the x axis between .805 and .845 nm.

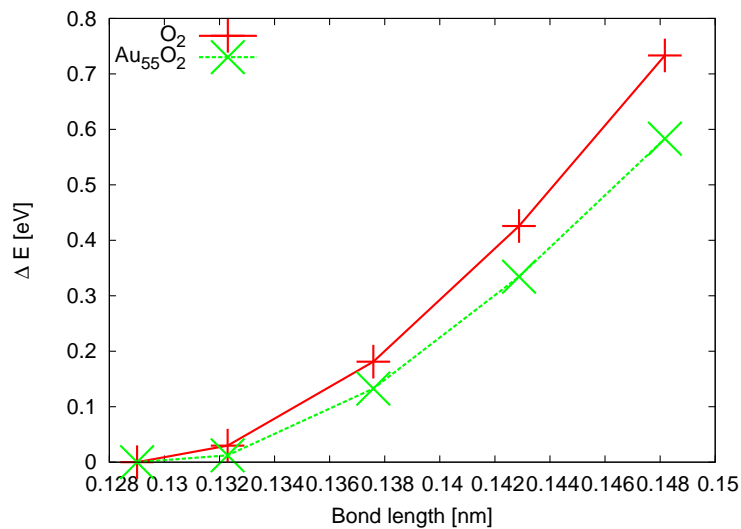


Figure 10: Difference in energy from the lowest energy state as a function of the distance between the two oxygen atoms.

-0.332135 eV.

More interesting from the point of catalysis is to fix the center of mass distance of the O_2 , vary the distance between the two oxygens and study the energy as a function of this bond length. This is shown in Figure 10 together with the energy as function of bond length for free standing O_2 not in the presence of the gold nanoparticle. Here we fixed the distance from the origin to the center of mass of the O_2 to be .815 nm. For all the data points that we studied in Figure 10 the presence of the Au_{55} nanoparticle lowered the energy and made the potential flatter as a function of separation of the two oxygens then would have been the case without the nanoparticle. This can be seen to give support to the idea that gold nanoparticle can be used to assist the breaking of O_2 , but from the figure the difference is small, less than .1 eV, so that more detailed studies are necessary to be definitive. One can also study the effect of different orientation of the O_2 with respect to the gold nanoparticle as this can effect the energy of the system as well as the binding of the O_2 , rather than bring in the O_2 along the x axis as we have done.

5 Conclusion

In this paper we have begun a study of the energy landscape for gold nanoclusters using density functional theory run on large parallel computers. By restricting ourselves to cuboctahedral and icosahedral geometries as well as intermediate geometries we have explored a small subspace of low energy gold nanostructures. We found that the cuboctahedral shape was lower energy than the icosahedral shape for 13 atoms and the opposite was the case for 55 and 147 atoms. We also estimated the energy difference. More significantly we were able to calculate the potential energy as a function of bond length and shape by introducing a shape parameter θ . Finally we were able to calculate the effect of the presence of nanogold on the binding energy of O_2 showing that it leads to weaker binding which may have applications for the use of nanogold for catalysis. In the future it will be interesting to expand the configuration space of geometries that can be efficiently probed for gold nanoclusters. Because the chemistry and material properties of these clusters depend strongly on geometry this is likely to have practical applications. Rapidly expanding computational resources dedicated to nanoscience indicates that this will be possible in the near future.

Acknowledgments

This manuscript has been authored in part by Brookhaven Science Associates, LLC, under Contract No. DE-AC02-98CH10886 with the U.S. Department of Energy.

References

- [1] P.D. Jadzinsky, G. Calero, C.J. Ackerson, D.A. Bushnell, R. D. Kornberg, “structure of a Thiol monolayer-protected gold nanoparticle at 1.1 Angstrom resolution”, *Science* 318, 430 (2007).
- [2] C. Fiolhais, F. Nogueira, M. Marques (eds.), *A Primer in Density Functional Theory* (Springer-Verlag, 2003).
- [3] E. J. Bylaska et al, ”NWChem, A Computational Chemistry Package for Parallel Computers, Version 5.1” (2007), Pacific Northwest National Laboratory, Richland, Washington 99352-0999, USA.
- [4] E. Apra, E. J. Bylaska, D. J. Dean, A. Fortunelli, F. Gao, P. S. Krsti, J. C. Wells and T. L. Windus, “NWChem for materials science”, *Computational Materials Science*, 28, 209 (2003).
- [5] Walter J. Stevens, Morris Krauss, Harold Basch, and Paul G. Jasien, “Relativistic compact effective potentials and efficient, shared-exponent basis sets for the third-, fourth-, and fifth-row atoms”, *Can. J. Chem.* 70, 612 (1992).
- [6] J.P. Perdew, S. Kurth, A. Zupan and P. Blaha, *Phys. Rev. Lett.* 82, 2544 (1999).
- [7] NWChem User Documentation release 5.1, <http://www.emsl.pnl.gov/docs/nwchem/nwchem.html>.
- [8] O. Haberen, S. Chung, M. Stener, and N. Rosch, “From clusters to bulk: A relativistic density functional investigation on a series of gold clusters Au_n , $n = 6, \dots, 147$ ”, *J. Chem. Phys.* 106, 5189 (1997).
- [9] J. Wang, G. Wang and J. Zhao, “Density-functional study of Au_n ($n = 2 - 20$) clusters: Lowest-energy structures and electronic properties”, *Phys. Rev. B* 66, 035418 (2002).
- [10] F. Baletto and R. Ferrando, “Structural properties of nanoclusters: Energetic, thermodynamic, and kinetic effects”, *Rev. of Mod. Phys.* 77, 371 (2005).
- [11] Y. Dong and M. Springborg, “Global structure optimization study on Au_{2-20} ”, *Eur. Phys. J. D* 43, 15 (2007).
- [12] M. Gruber, G. Heimel, L. Romaner, J. Bredas and E. Zojer, “First principles study of the geometric and electronic structure of Au_{13} clusters: Importance of the prism motif”, *Phys. Rev. B* 77, 165411 (2008).
- [13] A.S. Barnard et al, “Nanogold: A quantitative phase map”, *ACS nano* (2009).

- [14] H. Hakkinen, M. Moseler, “55-Atom clusters of silver and gold: Symmetry breaking by relativistic effects”, *Computational Materials Science* 35, 332 (2006).
- [15] W. Huang et al, “Relativistic effects and the unique low-symmetry structures of gold nanoclusters”, *ACS Nano*, 2, 897 (2008).
- [16] C.M. Wei, C. Cheng, C. M. Chang, “transition between icosahedral and cuboctahedral nanoclusters of lead”, *J. Phys. Chem. B* 110, 24642 (2006).
- [17] G. Rollmann et al, “Shellwise Mackay transformations in iron nanoclusters”, *Phys. rev. Lett.* 99, 083402 (2007).
- [18] T.P. Martin, “Shells of atoms”, *Physics Reports* 273, 199 (1996).
- [19] E. Apra, F. Baletto, R. Ferrando and A. Fortunelli, “Amorphization Mechanism of Icosahedral Metal Nanoclusters”, *Phys. Rev. Lett.* 93, 065502 (2004).
- [20] M.E. Gruner, G. Rollmann, A. Hucht, and P. Entel, “Massively parallel density functional theory calculations of large transition metal clusters”, *Lecture Series on Computer and Computational Sciences*
- [21] M.E. Gruner, G. Rollmann, P. Entel, “Large-scale first principles calculations of magnetic nanoparticles”, *NIC Series*, 39, 161 (2008).
- [22] M. Turner et al, “Selective oxidation with dioxygen by gold nanoparticle catalysts derived from 55-atom clusters”, *Nature* 07194, 981 (2008).
- [23] A. Roldan, S. Gonzalez, J. Ricart, and F. Illas, “Critical size O_2 dissociation by Au nanoparticles”, *ChemPhysChem* 11, 348 (2009).
- [24] H.G. Boyen et al, “Oxidation-resistant gold-55 clusters”, *Science* 297, 1533 (2002).
- [25] M. Okumura, Y. Kitagawa, M. Haruta, K. Yamaguchi, “The interaction of neutral and charged Au clusters with O_2 , CO and H_2 ”, *Applied Catalysis A: General* 291, 37 (2005).